J Nanopart Res (2018) 20: 196
https://doi.org/10.1007/s11051-018-4298-z

RESEARCH PAPER

In situ coating on $LiFePO_4$ with ionic liquid as carbon source for high-performance lithium batteries

Jun Xia · Fuliang Zhu · Lei Wang · Gongrui Wang · Yanshuang Meng · Yue Zhang

Received: 16 January 2018 / Accepted: 6 July 2018 / Published online: 17 July 2018

Abstract $LiFePO_4$/C materials were synthesized via an in situ coating on $LiFePO_4$ with 1-butyl-3-methylimidazolium dicyanamide [BMIm][$N(CN)_2$] as a carbon source. The electrode materials were characterized by X-ray diffraction (XRD), Fourier transform infrared (FTIR) spectra, Raman spectroscopy, scanning electron microscopy (SEM), and transmission electron microscopy (TEM). The results revealed that 1–2 nm carbon films were successfully coated on the $LiFePO_4$ particles. The electrochemical properties of $LiFePO_4$/C composite were investigated by cyclic voltammetry (CV) curves, electrochemical impedance spectra (EIS), and electrochemical analysis. The test results showed that the $LiFePO_4$/C composite possessed outstanding reversibility, cycle performance, and rate performance. The discharge capacities of $LiFePO_4$/C were 161.5 mAh g^{-1} at 0.1 C and 143.6 mAh g^{-1} at 1 C, respectively. The excellent electrochemical properties of the $LiFePO_4$/C electrode were mainly due to the thin, uniform, and highly graphitized carbon films.

J. Xia · F. Zhu · L. Wang · G. Wang · Y. Meng
School of Materials Science and Engineering, Lanzhou University of Technology, Lanzhou 730050, China

F. Zhu · Y. Meng (✉)
State Key Laboratory of Advanced Processing and Recycling of Non-ferrous Metals, Lanzhou 730050, China
e-mail: mengyanshuang@163.com

Y. Zhang (✉)
Department of Manufacturing Engineering, Georgia Southern University, Statesboro, GA 30460, USA
e-mail: yzhang@georgiasouthern.edu

Keywords In situ coating · Ionic liquid · Lithium ion batteries · $LiFePO_4$ · Electrochemistry · Energy storage

Introduction

Olivine structure lithium iron phosphate ($LiFePO_4$) has been the focus of an increasing number of research as cathode materials for lithium-ion batteries (LIBs) due to its high theoretical capacity, excellent thermal stability, high energy density, low cost, and non-toxicity. However, the widespread applications of $LiFePO_4$ cathode are hindered by its inherent low electronical conductivity and low Li^+ diffusion coefficient (Zhang et al. 2010). There have been a large number of investigations to improve the electronical and Li^+ conductivity of $LiFePO_4$, including reducing the particle size of $LiFePO_4$ (Chang et al. 2014; Li et al. 2014a), optimizing the morphology (Liu et al. 2011; Sun et al. 2011), decorating the surface with the conductive agent (Lei et al. 2009; Wang et al. 2008), and doping the high valence cation (Ding and Zhang 2012; Pei et al. 2011; Zhang et al. 2012). Among these strategies, carbon coating is the most effective one because the carbon films not only improve the surface conductivity but also prevent the dissolution and migration of irons, which, in return, significantly improve the reversibility, capacity, cycle stability, and rate performance of LIBs (Wang et al. 2013a; Yang et al. 2013). Previous studies have reported that, in a large extent, the thickness and uniformity of carbon films determine the electrochemical performance of the carbon-coated electrode (Ait Salah et al.

2006; Li and Zhou 2012; Li et al. 2014b; Wang and Sun 2012). The work carried out by Dominko and Cho both have demonstrated that the thickness of carbon films played a critical role in determining the capacity of $LiFePO_4$ cathode and thinner carbon films were more desired (Cho et al. 2009; Dominko et al. 2005). Cho and coworkers also found that the uniformity of carbon films in $LiFePO_4$/C was a crucial parameter in determining the electrochemical performance (Cho et al. 2009).

Many methods have been used to synthesis $LiFePO_4$/C materials, including hydrothermal method (Lin et al. 2014; Su et al. 2012; Wang et al. 2013c), solid-state reactions (Hu et al. 2011; Zhao et al. 2010), microwave synthesis (Chen et al. 2014), spray drying, and solvothermal process (Guo et al. 2013; Ren et al. 2013a; Wang et al. 2013b; Zhou et al. 2013). Of these methods, the carbon coating mechanism can be divided into two groups: (1) in situ growth and (2) postannealing. For in situ growth, the $LiFePO_4$ and carbon films are generated simultaneously by heating the mixture of the precursors of $LiFePO_4$ and carbon. While for postannealing, the carbon precursor is mixed with $LiFePO_4$ and then heated to produce carbon films. Currently, the most cost-effective method for large-scale production is the in situ growth as most of the postannealing methods require long-term annealing, high temperature, special equipment, or expensive raw materials.

Previous researches indicated that the carbon precursors play an important role in determining the morphology of the coated carbon film and the electrochemical performance of $LiFePO_4$ (Chen et al. 2016). Zhang and coworkers introduced an in situ synthesis method for $LiFePO_4$/C using asphalt as carbon precursor (Wang and Dai 2010). The obtained carbon films were unevenly coated on the $LiFePO_4$ particles. Chen et al. used poly(furfuryl alcohol) as carbon precursor to prepare $LiFePO_4$/C with porous structure. The obtained carbon film was not uniform and the discharge retention was 93% at 0.5 C after 50 cycles (Chen et al. 2016).

To improve the quality of carbon films, many materials have been studied as carbon precursors (Liang et al. 2008; Ni et al. 2010; Wang and Dai 2010). Among these materials, ionic liquids (ILs) have attracted numerous interests as carbon precursor due to many of their beneficial properties, such as low viscosity, excellent liquidity, low vapor pressure, and high thermal stability (Ma et al. 2010). Our previous work indicate that the ILs have good wettability on $LiFeO_4$ surface, which benefits the penetration of ILs into the pores of $LiFePO_4$ particles, facilitating the formation of uniform and tightly bonded carbon films on $LiFePO_4$ particles (Meng et al. 2017). More importantly, ILs can introduce doped heteroatoms to the carbon films which can enhance the electrode/electrolyte wettability, the reactivity, the electronical conductivity and, therefore, the electrochemical performance (Li et al. 2009; Liu et al. 2015; Qie et al. 2012; Ren et al. 2013b). In our previous work, nitrogen-doped carbon (NDC) was obtained by pyrolyzing IL, in which the nitrogen dopant created large number active sites for Li^+ ion adsorption, thus could greatly improve the specific capacity of the carbon material (Meng et al. 2017; Meng et al. 2016; Xia et al. 2017).

In this work, we have produced carbon film-coated $LiFePO_4$ by using in situ hydrothermal method. To our best knowledge, this is the first time that ionic liquid material was used as carbon precursor in this in situ hydrothermal method. The synthesized $LiFePO_4$/C was first characterized by a variety of techniques including XRD spectroscopy, FTIR spectroscopy, Raman spectroscopy, and TEM microscopy. The uniformly coated carbon films had a thickness of 1–2 nm, which was rarely reported before. The material was assembled into coin type half-cells to measure the electrochemical properties. The obtained $LiFePO_4$/C electrode displayed excellent reversibility, outstanding cycle stability, superior rate performance, and remarkable charge–discharge capacity. The improved electrochemical performance of the $LiFePO_4$/C electrode can be attributed to the special carbon film structure which shortens the electron path between $LiFePO_4$ particles. These results indicate that ILs are suitable carbon precursor for the in situ hydrothermal synthesis of $LiFePO_4$/C materials which show promising applications in energy storage devices.

Experimental

Synthesis of carbon-coated $LiFePO_4$ cathode materials

In a typical synthesis process, the stoichiometric amounts of $LiOH{\cdot}H_2O$ (98%), H_3PO_4 (85%), and $FeSO_4{\cdot}7H_2O$ (99%) (molar ratio is 3:1:1) were dissolved in distilled water respectively. Afterwards, ionic liquid [BMIm][$N(CN)_2$] (30 wt%) was added into mixed solution with vigorous stirring for 30 min. And then the mixture was transferred to a 200-mL Teflon-

lined stainless steel autoclave and maintained at a temperature of 180 °C for 10 h. After cooling to room temperature, the obtained gray dark slurry was centrifuged, poured out the upper suspension, washed several times with distilled water and alcohol, and finally dried at 110 °C for 12 h to get the mixture of $LiFePO_4$ (before annealing denoted as LFP/CB). Then, the mixture was dried and calcined in an argon atmosphere. The temperature starts at 50 to 300 °C (5 °C per minute) keeping warm for 2 h and heated to 700 °C in the same rate. During cooling down to the room temperature, carbon-coated $LiFePO_4$ samples (after annealing denoted as LFP/CA) were obtained.

Structural and morphology characterization

XRD characterization for LFP/CA and LFP/CB were investigated using a Rigaku D/max-2500 with Cu Kα radiation. Elemental analysis was collected with an Elementar Analysensysteme GmbH varioEL cube. FTIR spectra of samples were measured on a Nexus 670 FTIR spectrometer. Raman spectra were obtained from a LabRAM HR UV/vis/NIR (Horiba Jobin Yvon, France). The SEM images and EDS spectra were obtained by using a scanning electron microscope (JEOL-7500F) with EDS device. TEM were carried out with a transmission electron microscopy (JEOL JEM-2010F) equipment. The electronic conductivity of the carbon-coated $LiFePO_4$ (before/after annealing) was investigated by a RTS-9 four-point probe resistivity measurement system.

Electrochemical characterization

Coin type half-cells (model 2032) were performed in the electrochemical test. Firstly, the working electrodes were prepared by using LFP/CB and LFP/CA as the active materials, polyvinylidene fluoride (PVDF) binder, and conductive carbon blacks (Super-P) in a weight ratio of 8:1:1. They were mixed in a mortar for 5 min and then dispersed in *N*-methyl-pyrrolidone (NMP) and coated onto an aluminum foil. Secondly, the solvent was coated onto Al foil and evaporated at 110 °C for 10 h under vacuum drying box. Half-cells were assembled inside the glove box using 1 M $LiPF_6$ in a mixture of EC:DEC (1:1 vol%). For electrochemical testing, the half-cells were charged and discharged constant current within a fixed voltage window between 2.5 and 4.2 V (with the same charge–discharge rates). The charge–discharge cycling studies of the cells were calculated by Land CT2001A. Cyclic voltammetry (CV) was performed with an electrochemical workstation (Chi660E, Shanghai Chenhua instruments) at a scan rate between 0.1 and 0.2 mV s^{-1}. Electrochemical impedance spectra (EIS) were measured in the frequency range from 0.01 Hz to100 kHz. All cells were tested at room temperature.

Results and discussion

The formation mechanism of LFP/CA is further investigated and the schematic illustration is shown in Fig. 1. First, the small primary nanoparticles begin to assemble together which involves a short nucleation and the following crystal growth progress (Deng et al. 2012b; Guo et al. 2013). At the same time, the $[BMIm][N(CN)_2]$ is free from the bondage of the Coulombic forces and ionized into $[BMIm]^+$ and $N(CN)_2^-$. Then, $[BMIm]^+$ is decomposed into methyl and butyl groups, while $[N(CN)_2]^-$ is decomposed into triazine ring. These chemical groups are carbonized at a low temperature of 180 °C. Since there is a disordered layer on the surface of LFP/CB, if it is not calcined at high temperature, the disordered layer will affect its capacity. Finally, the LFP/CB is completely carbonated after further annealing at high temperature.

The XRD patterns of LFP/CB and LFP/CA are shown in Fig. 2. Both samples display the characteristic peaks of $LiFePO_4$ which match well with the standard pattern (Zheng et al. 2015). The strong and sharp peaks indicate a high degree of crystallinity of the as-prepared $LiFePO_4$ (Xue et al. 2014). No diffraction peaks of Fe_2P, Fe_3P, or Li_3PO_4, which are usually observed in $LiFePO_4$ products, are observed, indicating a high purity of the synthesized $LiFePO_4$ (He et al. 2014; Hu et al. 2011; Long et al. 2014). The elemental analysis shows that carbon content is only 1.38%; therefore, the diffraction peak of carbon is not seen in the XRD patterns of LFP/CB and LFP/CA, which may be due to the low content of carbon in the samples (Liu and Wang 2014). Among the indexed peaks, three main peaks centered at 25.6°, 29.9°, and 35.7°, can be attributed to the (111), (121), and (131) crystal planes of $LiFePO_4$, respectively (Wu et al. 2009). These results reflect that in situ coating on $LiFePO_4$ by using $[BMIm][N(CN)_2]$ as a carbon source can produce $LiFePO_4$ with the high crystallinity and

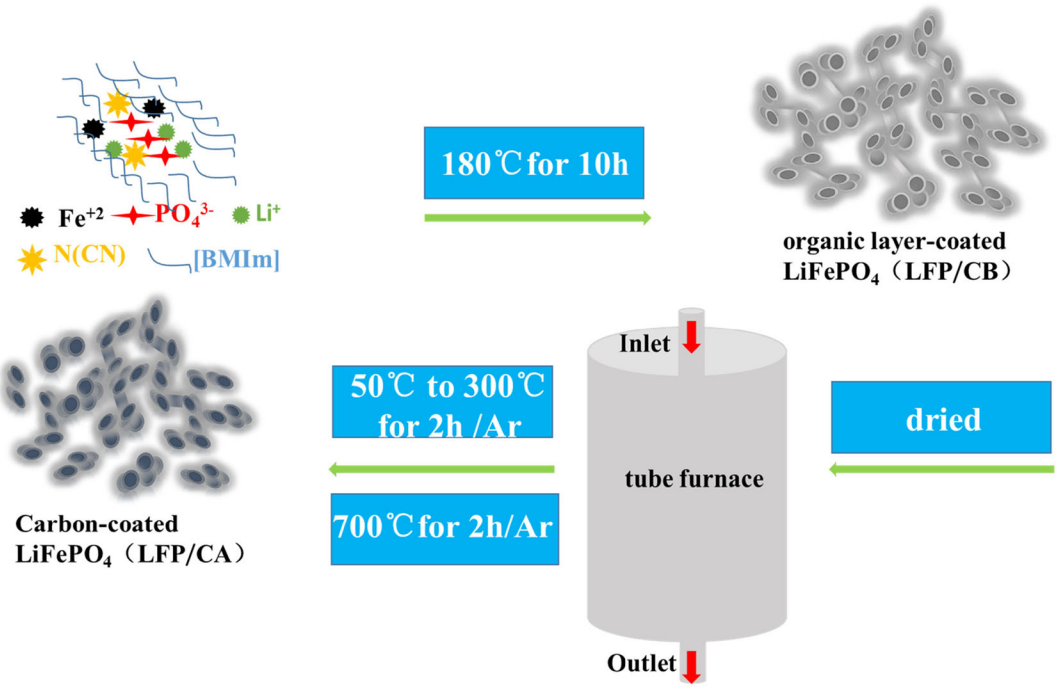

Fig. 1 Schematic illustration of the LFP/CA sample

purity, which are major factors for a high-performance electrode material.

The FTIR spectra are used to investigate the changes of chemical groups from IL to LFP/CB and LFP/CA. Figure 3 exhibits the FTIR spectra of ILs, LFP/CB, and LFP /CA. The peak of ILs at 3445 cm^{-1} is due to the absorbed moisture in the $[BMIm][N(CN)_2]$, which is also observed in the spectra of LFP/CB and LFP/CA[45]. The peaks at 3140 cm^{-1} is caused by the stretching vibrations of aromatic C–H. The $[BMIm][N(CN)_2]$ have three main bands at 2941, 2873, and 1310 cm^{-1} which stem from the asymmetric and symmetric stretching vibrations of aliphatic C–H bonds[46]. Bands from 2235 to 2140 cm^{-1} are due to the stretching vibrations of C≡N in the anion $[N(CN)_2]^-$. The peak at 746 cm^{-1} is attributed to the deformation of C–H bonds. After the heat treatment, the peaks at 3140, 2941, 2873, 2235, 2140, 1310, and 746 cm^{-1} disappear, indicating the decomposition of methyl and butyl groups and the break of C≡N chemical bonds. The strong absorption peaks of LFP/CB and LFP/

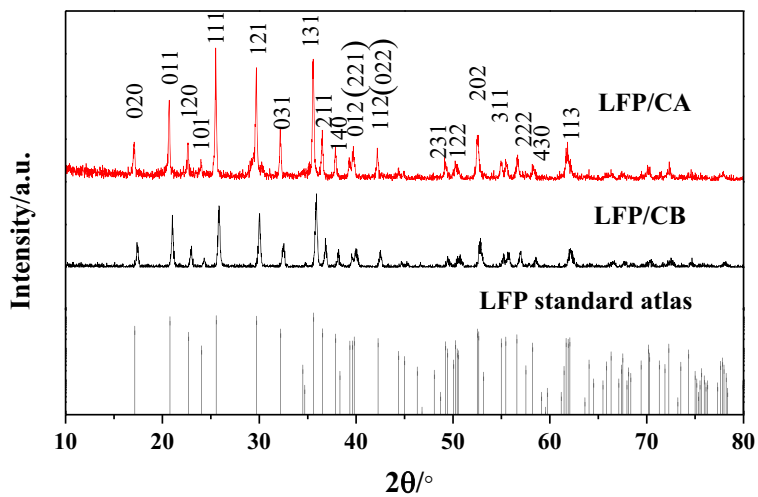

Fig. 2 XRD patterns of LFP/CB, LFP/CA, and LFP standard atlas

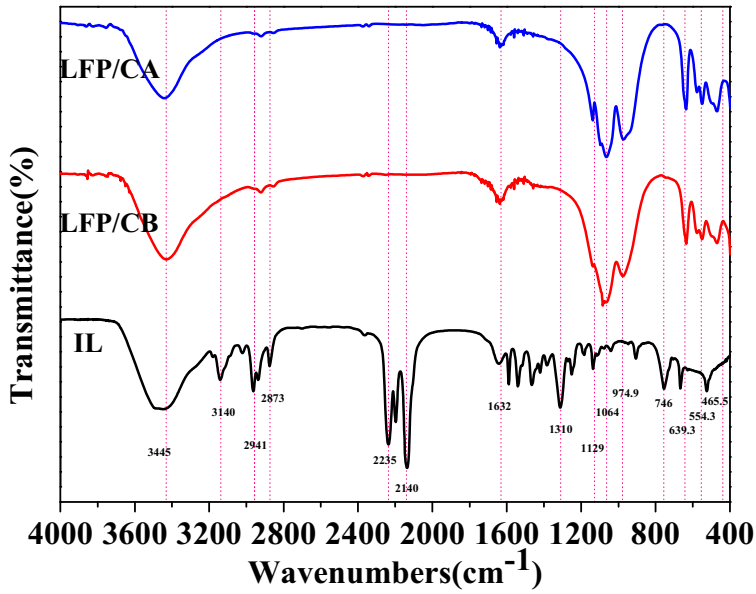

Fig. 3 FTIR spectra of IL, LFP/CB, and LFP/CA

CA appear at 1129, 1064, and 974.9 cm^{-1}, corresponding to the bending modes of the $(PO_4)^{3-}$ (Lepage et al. 2011). The peaks in the range of 639.3 to 465.5 cm^{-1} raise from the asymmetric bending of O–P–O (Kumar et al. 2011). All these vibrations bands are the main peaks of $LiFePO_4$, indicating the formation of $LiFePO_4$. Moreover, the absorption peak at 1632 cm^{-1} is due to the symmetrical stretching of sp^2-type bonding of C=C (Cho et al. 2009; Kumar et al. 2011; Xie et al. 2006). The LFP/CB sample exhibits the peaks of sp^2 carbon, indicating that the $[BMIm][N(CN)_2]$ has been carbonized at a pretty low temperature of 180 °C.

Raman spectra of the LFP/CB and LFP/CA, as shown in Fig. 4, are used to analyze the carbon microstructure (Ma et al. 2015). It is found that a strong Raman peak of the LFP/CB and LFP/CA around 947 cm^{-1} is attributed to the symmetric vibration of the PO_4 group which is detected for the pure $LiFePO_4$ (Liang et al. 2013; Ma et al. 2015; Nakano et al. 2008). This result is further proof that we have synthesized the pure $LiFePO_4$ and which is in good agreement with XRD patterns and FTIR results. The bands of LFP/CA, located in the range of 1358 and 1593 cm^{-1} stem from D-band (the A_{1g} vibration of the disordered carbon) and G-band (the E_{2g} vibration the graphitic carbon), respectively (Deng et al. 2012a; Deng et al. 2012b). The intensity ratio of D-band to G-band (I_D/I_G) is 0.89; the smaller the I_D/I_G ratio, the higher the degree of graphitic carbon (Shi et al. 2012). More importantly, graphitization carbon can improve the electrochemical performance of LFP/CA (Jin et al. 2011; Tang et al. 2013; Xu et al. 2015; Xu et al. 2016). Because the $[BMIm][N(CN)_2]$ are incomplete carbonization in LFP/CB, there is a broad D-band and obvious G-band. The broad D peak means a higher degree of disordered carbon (Shin et al. 2001). After annealing, the broad D-band becomes more obvious and exhibits a sharp G-band. More importantly, the graphitization degree has increased and the ratio of disordered carbon has decreased tremendously. As expected, all the results indicate that the surface of LFP/CA particles is coated by carbon which comes from pyrolysis of $[BMIm][N(CN)_2]$.

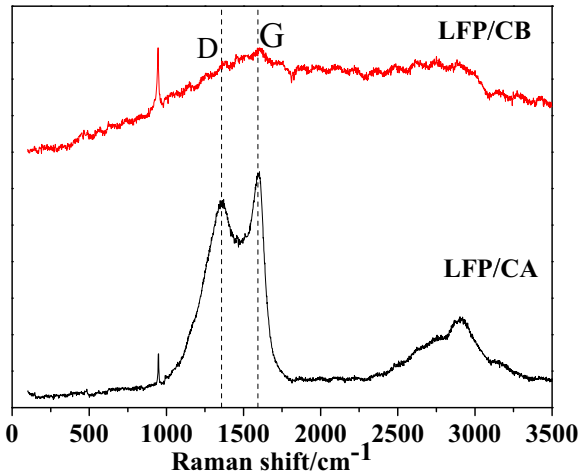

Fig. 4 Raman spectrum of the LFP/CB and LFP/CA

Figure 5a–d shows the SEM images of LFP/CB and LFP/CA. The average particle size of LFP/CB and LFP/CA samples are ~ 200 nm, which are confirmed by the TEM image (Fig. 6). The results indicate that the microstructures of the globular LFP/CB are stable enough that they cannot be destroyed even after high-temperature treatment. Furthermore, compared with LFP/CB sample, the morphology of LFP/CA sample is more regular.

Figure 5e, f shows the main elements of LFP/CB and LFP/CA, which include C, O, Fe, and P. The C is the main element generated by the thermal pyrolysis of IL. The O, Fe, and P are the main elements of LFP, and the low intensity of C indicates a low content of carbon in LFP/CB and LFP/CA samples.

The TEM images, seen in Fig. 6, show the morphology of LFP/CB and LFP /CA. In Fig. 6a, b, d, e,

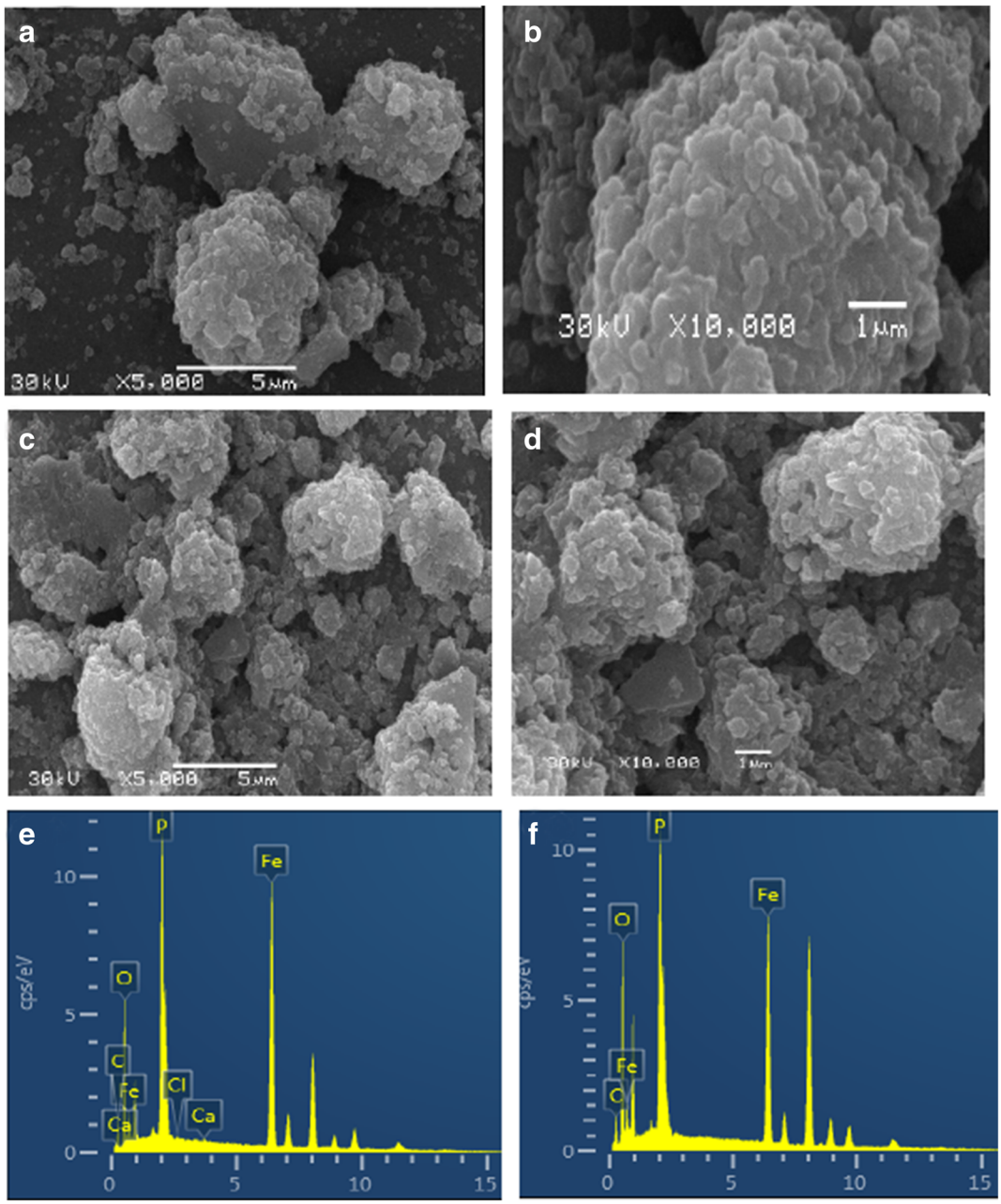

Fig. 5 SEM images LFP/CB (**a**, **b**), LFP/CA (**c**, **d**), and EDX spectra of LFP/CB and LFP/CA (**e**, **f**)

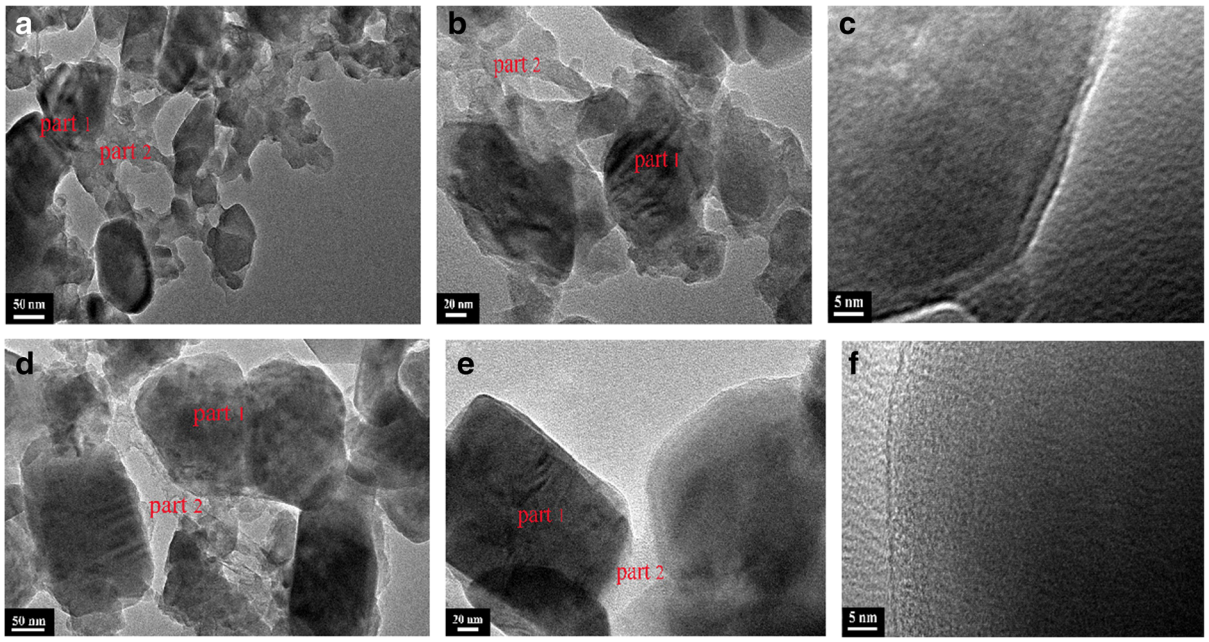

Fig. 6 TEM images LFP/CB (**a**–**c**) and LFP/CA (**d**–**f**)

$LiFePO_4$ particles appear in dark particles (part 1) and the carbon materials appear in light layers (part 2). These carbon materials filled the gap and voids between $LiFePO_4$ particles, which provides more interface area between the electrolyte and electrode material, and this facilitates the penetration of electrolyte into electrode particles, thus improving the electronic conductivity of the $LiFePO_4$ particles (Chen et al. 2015). A close look of the $LiFePO_4$ particles shows carbon films of 1–2 nm that tightly coat on the $LiFePO_4$ particles (Fig. 6c, f). As $[BMIm][N(CN)_2]$ has good wettability on $LiFePO_4$, which facilities the penetration of the ionic liquid into the pores of $LiFePO_4$ particles, strong interface is formed between the coated carbon film and the $LiFePO_4$ particles after the thermal pyrolysis of $[BMIm][N(CN)_2]$. The thin and uniform carbon films can accelerate the migration of Li^+ ions, and because of this, the coated carbon films can improve the rate capacity of $LiFePO_4$ (Long et al. 2014). The TEM analysis indicates that the carbon films are uniformly coated on the $LiFePO_4$ particles and also bridge these particles, which could contribute to the electronic conductivity, thus increasing the electrochemical performance.

To investigate the electrochemical performance of LFP/CB and LFP/CA, coin type half-cells is assembled. Figure 7a shows the CV curves of LFP/CA at 0.1, 0.5, and 1.0 mVs^{-1} over the potential range of 2.5–4.2 V. The potential intervals between redox peaks are 0.29, 0.54, and 0.72 V at the scan rate of 0.1, 0.5, and 1.0 mVs^{-1}, respectively. When the scan rate increases, the potential interval becomes broader. Moreover, the symmetrical redox peaks suggest an excellent kinetics of LFP/CA. The electronic conductivity of the carbon-coated $LiFePO_4$ (before/after annealing) was investigated by a four probe conductivity system. The electronic conductivity of the LFP/CB is 7.63×10^{-5} S cm^{-1}, while the LFP/CA sample is 1.37×10^{-1} S cm^{-1}. Obviously, the in situ coating technology has the low polarization. What's more, it is expected that the LFP/CA prepared through in situ coating on $LiFePO_4$ by using $[BMIm][N(CN)_2]$ as a carbon source will have enhanced electrochemical properties, such as rate performance and circulation property.

As showed from Fig. 7b, in contrast to the LFP/CB, the oxidation reduction peaks of LFP/CA are more symmetrical and sharper shape, indicating high electrochemical reversibility of the Li^+ intercalation/deintercalation (Zheng et al. 2015). The electronic conductivity of the LFP/CA is enhanced due to the carbon films of the LFP/CA, which serves as the protective layer, thus limiting the decomposition of LFP particles during the cycling process. For LFP/CA, the oxidation peak and the reduction peak are at around 3.57 and 3.29 V, which correspond to Li^+ insertion/extraction.

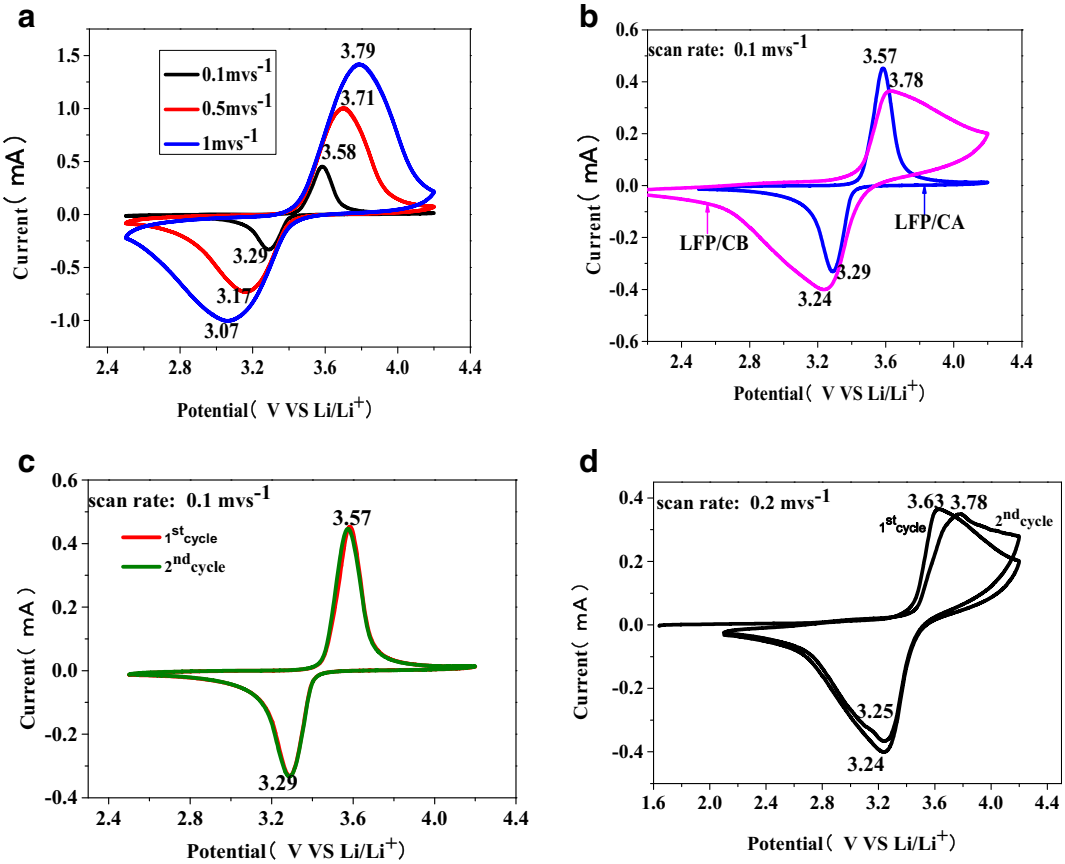

Fig. 7 **a** CV profiles of LFP/CA with different scan rates. **b** CV curves of LFP/CB and LFP/CA at a scan rate of 0.1 mVs^{-1}. **c** First two-cycle CV behavior of LFP/CA. **d** First two-cycle CV behavior of LFP/CB

Furthermore, the separation potential of LFP/CA between the oxidation peak and the reduction peak is 0.28 V, whereas that of the LFP/CB is 0.54 V. This indicates that the LFP/CA samples have an excellent electrode kinetics and lower electrode polarization, which are consistent with the results of the other groups (Deng et al. 2012a; Jiang et al. 2015; Sun et al. 2012). According to the previous results of Raman spectroscopy, the smaller separation potential may be attributed to the higher electronic conductivity of graphitic carbon (Liang et al. 2013).

Figure 7c, d exhibits the CV curves of the LFP/CA and LFP/CB by using a scan rate of 0.1 mVs^{-1} for the first two cycles. From Fig. 7c, in contrast to the LFP/CB, the good overlap of the redox peak in the first two cycles indicates that the electrode of LFP/CA is stable (Luo et al. 2010).

Figure 8a shows charge–discharge curves of the LFP/CA and LFP/CB samples for the first cycle at a 0.1 C rate. It is clearly indicative from the figure that the reversible first discharge capacity of LFP/CA sample reaches 161.5 mAh g^{-1} (the coulombic efficiency is 98.6%), while the discharge capacity of LFP/CA sample is 62.4 mAh g^{-1} (the coulombic efficiency is 87.3%). Moreover, the polarization potential of the LFP/CA sample is much better than that of LFP/CB sample. The main reason is the decrease of potential interval (ΔE) from 150 mV (LFP/CB) to 100 mV (LFP/CA). This is attributed to the thin, uniform, and highly graphitized carbon films derived from $[BMIm][N(CN)_2]$ coated on the $LiFePO_4$ particles, which can enhance the surface electronic conductivity, thus alleviating the electrode polarization. Figure 8b displays the first, tenth, twentieth, and fiftieth cycles profiles of the LFP/CA sample at a 0.1 C rate. It can be seen that LFP/CA sample still has super charge–discharge (161.9/160.6 mAh g^{-1}) stability, even after 50 cycles, which is due to the electronic conductivity of $LiFePO_4$ that has been improved by the thin and highly graphitized carbon films.

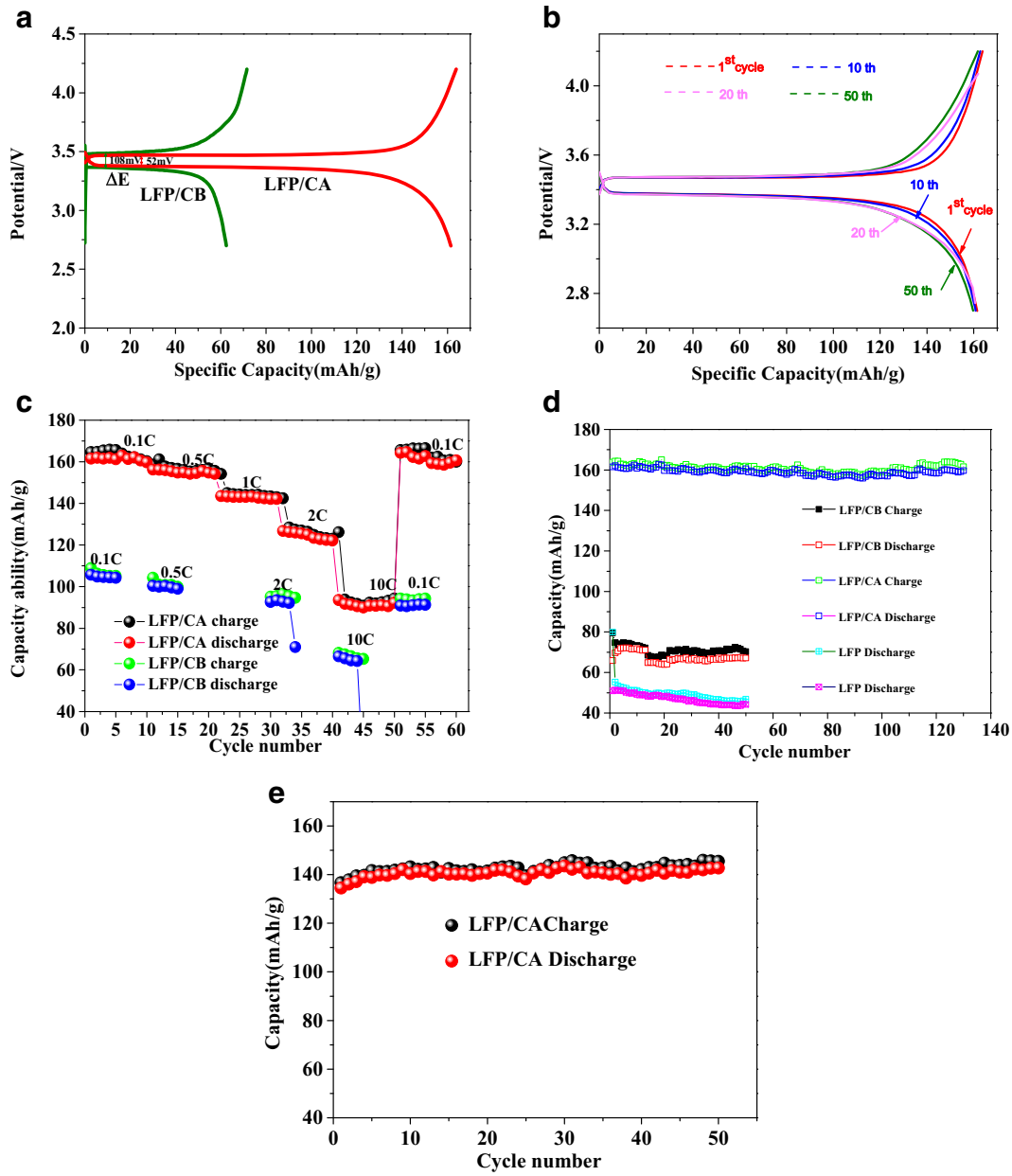

Fig. 8 **a** Charge and discharge curves of the LFP/CA and LFP/CB samples at a 0.1 C rate for the first cycle. **b** The first, tenth, twentieth, and fiftieth cycle profiles of the LFP/CA sample at a 0.1 C rate. **c** Rate capability of LFP/CA. **d** Cycling performance of LFP/CA, LFP/CB and LFP at 0.1 C rate. **e** Cycling performance of LFP/CA at 1 C rate

The rate capabilities of the LFP/CA sample at the rates of 0.1, 0.5, 1, 2, and 10 C are shown in Fig. 8c. From 0.1 to 2 C, the capacity loss of the LFP/CA sample is only 19.8%. Even though at a high rate of 10 C, LFP/CA material still has a high capacity of 93.7 mAh g^{-1}, which shows its excellent rate capability. What's more, when the rate returns to 0.1 C, the LFP/CA sample has a discharge capacity of 164.3 mAh g^{-1}. The results indicate that the LFP/CA sample has high electrochemical reversibility, which are consistent with the CV measurement results.

Figure 8d shows the cycle capacity of LFP/CA, LFP/CB, and LFP (before annealing) samples under the 0.1 C rate. It can be found from Fig. 7d that the discharge capacity of LFP/CA sample is 161.5 mAh g^{-1} in the first cycle and remained 159.7 mAh g^{-1} after 130 cycles at

0.1 C. And yet, the performance of LFP/CB is low and decreases with the cycle number. While the he initial discharge capacity of LFP sample is only 50.9 mAh g^{-1}.The reason for that is because the disordered carbon layer of LFP/CB has bad electric conductivity. Another reason is because LFP/CB particles have a disordered surface layer, which will result in an increase of the electric resistance. While for LFP sample, the carbon films inhibit the growth of LFP particles, which, in turn, reduces the path of Li^+ insertion and deinsertion. Therefore, the structure of the active material should be an important factor affecting the performance of the discharge capacity and cycling stability. The experimental results show that LFP/CA synthesized by in situ coating on $LiFePO_4$ using [BMIm][$N(CN)_2$] as a carbon source has good electrochemical performances. Figure 7e shows the high rate cycle capacity of LFP/CA sample under the 1 C rate. The initial discharge capacity of LFP/CA sample is 135.2 mAh g^{-1} in the first cycle and remained 143.2 mAh g^{-1} even after 50 cycles at 1 C.

Figure 9 shows AC impedance measurements of LFP/CB and LFP/CA, which are in order to further analyze the dynamic characteristic of the samples. It is noted that the semicircles are related to the charge transfer resistance between the electrolyte and the active material. The slope lines are attributed to Warburg impedance in the lower frequency. The former is caused by charge transfer progress, while the latter is caused by Li^+ diffusion in $LiFePO_4$ electrode (Liu et al. 2009; Pei et al. 2011; Wang and Dai 2010). The charge transfer resistance of LFP/CB (233.5 Ω) is far more than that of LFP/CA (74.2 Ω). Moreover, LFP/CA line slope in low frequency is much smaller than that of LFP/CB, indicating the lower Warburg impedance (Pei et al. 2011).

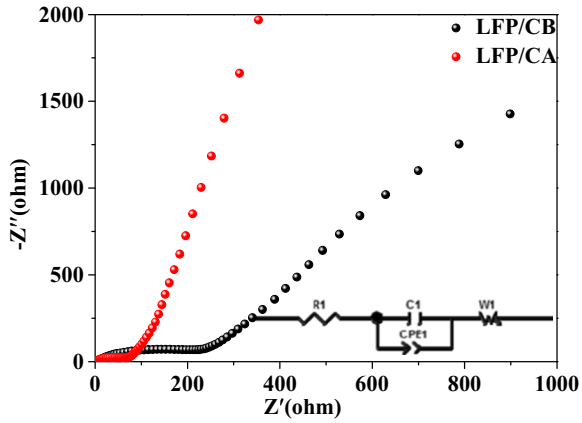

Fig. 9 EIS of LFP/CB and LFP/CA (inset: equivalent circuit)

AC impedance spectra is applied on the basis of equivalent circuit displayed in the inset of Fig. 8. The impedance spectra can be explained on the basis of an equivalent circuit with the charge transfer resistance (R2), Warburg impedance (W1), the double layer (CPE1), and the ohmic resistance (R1) (Xia et al. 2011). The results indicate that total electric resistance of LFP/CA is decreased by conductive carbon films coating. It is for this reason that the high electronic conductivity of the $LiFePO_4$ by coating carbon films and the efficient contact between electrochemical active particles.

Conclusions

In summary, we have elaborated a method for the preparation of LFP/CA sample by in situ coating on $LiFePO_4$ by using [BMIm][$N(CN)_2$] as a carbon source. Based on the FTIR, Raman, SEM, and TEM results, the ILs are free from the bondage of the coulomb force to split into $[BMIm]^+$ and $[N(CN)_2]^-$; then, $[BMIm]^+$ is decomposed into methyl and butyl groups and $[N(CN)_2]^-$ is decomposed into triazine ring. After annealing, the LFP/CB is then completely carbonated and the graphitization degree has increased and the ratio of disordered carbon has decreased tremendously. The sample shows excellent charge–discharge capacity of 163.8/161.5 mAh g^{-1} in the first cycle and remained 161.6/159.7 mAh g^{-1} after 130 cycles at 0.1 C. The LFP/CA sample also has superb rate capabilities. Even at a high current density of 10 C, LFP/CA material still has a high capacity of 93.7 mAh g^{-1}. The outstanding electrochemical performance is attributed to the thin, uniform, and highly graphitized carbon films (only 1–2 nm). It creates electron paths, thus greatly increase the electronic conductivity of LFP/CB. Moreover, the high-graphitized carbon films can transport the Li^+ with a high speed during charge–discharge process. Our results prove that [BMIm][$N(CN)_2$] is a perfect carbon source for the preparation of LFP/CA cathode materials with high electrochemical performance. Therefore, in situ coating on $LiFePO_4$ by using [BMIm][$N(CN)_2$] as a carbon source provides a novel and facile method for electrochemical energy storage.

Funding information This study received financial support from the National Nature Science Foundation of China (NFSC) (grant nos. 51364024, 51404124), Natural Science Foundation of

Gansu Province (grant no. 1506RJZA100), and the Foundation for Innovation Groups of Basic Research in Gansu Province (no. 1606RJIA322).

Compliance with ethical standards

Conflict of interest The authors declare that they have no conflict of interest.

References

Ait Salah A et al (2006) Reduction Fe[sup 3+] of impurities in LiFePO[sub 4] from pyrolysis of organic precursor used for carbon deposition. J Electrochem Soc 153:A1692. https://doi.org/10.1149/1.2213527

Chang Y-C, Peng C-T, Hung IM (2014) Effects of particle size and carbon coating on electrochemical properties of $LiFePO_4$/C prepared by hydrothermal method. J Mater Sci 49:6907–6916. https://doi.org/10.1007/s10853-014-8395-9

Chen R, Wu Y, Kong XY (2014) Monodisperse porous $LiFePO_4$/C microspheres derived by microwave-assisted hydrothermal process combined with carbothermal reduction for high power lithium-ion batteries. J Power Sources 258:246–252. https://doi.org/10.1016/j.jpowsour.2014.02.068

Chen M, Wang X, Shu H, Yu R, Yang X, Huang W (2015) Solvothermal synthesis of monodisperse micro-nanostructure starfish-like porous $LiFePO_4$ as cathode material for lithium-ion batteries. J Alloys Compd 652:213–219. https://doi.org/10.1016/j.jallcom.2015.08.221

Chen J et al (2016) Superior performance of $LiFePO_4$/C with porous structure synthesized by an in situ polymerization restriction method for lithium ion batteries. Mater Chem Phys 180:244–249. https://doi.org/10.1016/j.matchemphys.2016.06.002

Cho Y-D, Fey GT-K, Kao H-M (2009) The effect of carbon coating thickness on the capacity of $LiFePO_4$/C composite cathodes. J Power Sources 189:256–262. https://doi.org/10.1016/j.jpowsour.2008.09.053

Deng H, Jin S, Zhan L, Qiao W, Ling L (2012a) Nest-like $LiFePO_4$/C architectures for high performance lithium ion batteries. Electrochim Acta 78:633–637. https://doi.org/10.1016/j.electacta.2012.06.059

Deng H, Jin S, Zhan L, Wang Y, Qiao W, Ling L (2012b) Synthesis of cage-like $LiFePO_4$/C microspheres for high performance lithium ion batteries. J Power Sources 220:342–347. https://doi.org/10.1016/j.jpowsour.2012.07.060

Ding Y-h, Zhang P (2012) Effect of Mg and Co co-doping on electrochemical properties of $LiFePO_4$. Trans Nonferrous Metals Soc China 22:s153–s156. https://doi.org/10.1016/s1003-6326(12)61701-4

Dominko R, Bele M, Gaberscek M, Remskar M, Hanzel D, Pejovnik S, Jamnik J (2005) Impact of the carbon coating thickness on the electrochemical performance of LiFePO[sub 4]/C composites. J Electrochem Soc 152:A607. https://doi.org/10.1149/1.1860492

Guo J, Chen L, Zhang X, Chen H, Tang L (2013) Template-free solvothermal synthesis of monodisperse porous $LiFePO_4$ microsphere as a high-power cathode material for lithium-ion batteries. Mater Lett 106:290–293. https://doi.org/10.1016/j.matlet.2013.05.044

He J, Wang H, Gu C, Liu S (2014) Characterization and electrochemical performances of MoO_2 modified $LiFePO_4$/C cathode materials synthesized by in situ synthesis method. J Alloys Compd 604:239–244. https://doi.org/10.1016/j.jallcom.2014.03.134

Hu C, Yi H, Fang H, Yang B, Yao Y, Ma W, Dai Y (2011) Suppressing Li_3PO_4 impurity formation in $LiFePO_4$/Fe_2P by a nonstoichiometry synthesis and its effect on electrochemical properties. Mater Lett 65:1323–1326. https://doi.org/10.1016/j.matlet.2011.01.074

Jiang Y et al (2015) Synthesis and characterization of oriented linked $LiFePO_4$ nanoparticles with fast electron and ion transport for high-power lithium-ion batteries. Nano Res 8:3803–3814. https://doi.org/10.1007/s12274-015-0879-7

Jin Y, Yang CP, Rui XH, Cheng T, Chen CH (2011) V_2O_3 modified $LiFePO_4$/C composite with improved electrochemical performance. J Power Sources 196:5623–5630. https://doi.org/10.1016/j.jpowsour.2011.02.059

Kumar PR, Venkateswarlu M, Misra M, Mohanty AK, Satyanarayana N (2011) Carbon coated LiMnPO[sub 4] nanorods for lithium batteries. J Electrochem Soc 158:A227. https://doi.org/10.1149/1.3527059

Lei G, Yi X, Wang L, Li Z, Zhou J (2009) An investigation of the electrochemical performance of polyaniline coated LiFePO4materials. Polym Adv Technol 20:576–580. https://doi.org/10.1002/pat.1386

Lepage D, Michot C, Liang G, Gauthier M, Schougaard SB (2011) A soft chemistry approach to coating of $LiFePO_4$ with a conducting polymer. Angew Chem Int Ed 50:6884–6887. https://doi.org/10.1002/anie.201101661

Li H, Zhou H (2012) Enhancing the performances of Li-ion batteries by carbon-coating: present and future. Chem Commun (Camb) 48:1201–1217. https://doi.org/10.1039/c1cc14764a

Li X, Wang H, Robinson JT, Sanchez H, Diankov G, Dai H (2009) Simultaneous nitrogen doping and reduction of graphene oxide. J Am Chem Soc 131:15939–15944. https://doi.org/10.1021/ja907098f

Li D, Liu X, Zhou H (2014a) The size-dependent phase transition of LiFePO4 particles during charging and discharging in lithium-ion batteries. Energy Technology 2:542–547. https://doi.org/10.1002/ente.201300159

Li J, Zhang L, Zhang L, Hao W, Wang H, Qu Q, Zheng H (2014b) In-situ growth of graphene decorations for high-performance $LiFePO_4$ cathode through solid-state reaction. J Power Sources 249:311–319. https://doi.org/10.1016/j.jpowsour.2013.10.106

Liang G, Wang L, Ou X, Zhao X, Xu S (2008) Lithium iron phosphate with high-rate capability synthesized through hydrothermal reaction in glucose solution. J Power Sources 184:538–542. https://doi.org/10.1016/j.jpowsour.2008.02.056

Liang Y-P, Li C-C, Chen W-J, Lee J-T (2013) Hydrothermal synthesis of lithium iron phosphate using pyrrole as an efficient reducing agent. Electrochim Acta 87:763–769. https://doi.org/10.1016/j.electacta.2012.09.088

Lin M, Wu X, Chen BL, Yuan JK (2014) Hydrothermal synthesis of corn cob-like $LiFePO_4$/C as high performance cathode material for lithium ion batteries. Advances in Science and Technology, Trans Tech Publications, Switzerland 93:152–157. https://doi.org/10.4028/www.scientific.net/AST.93.152

Liu S, Wang H (2014) WO2 modified $LiFePO_4$/C cathode materials with improved electrochemical performance synthesized by in-situ synthesis method. Mater Lett 122:151–154. https://doi.org/10.1016/j.matlet.2014.02.017

Liu J, Jiang R, Wang X, Huang T, Yu A (2009) The defect chemistry of $LiFePO_4$ prepared by hydrothermal method at different pH values. J Power Sources 194:536–540. https://doi.org/10.1016/j.jpowsour.2009.05.007

Liu J, Conry TE, Song X, Doeff MM, Richardson TJ (2011) Nanoporous spherical $LiFePO_4$ for high performance cathodes. Energy Environ Sci 4:885–888. https://doi.org/10.1039/c0ee00662a

Liu X et al (2015) Nitrogen-doped 3D macroporous graphene frameworks as anode for high performance lithium-ion batteries. J Power Sources 293:799–805. https://doi.org/10.1016/j.jpowsour.2015.05.074

Long Y, Shu Y, Ma X, Ye M (2014) In-situ synthesizing superior high-rate $LiFePO_4$/C nanorods embedded in graphene matrix. Electrochim Acta 117:105–112. https://doi.org/10.1016/j.electacta.2013.11.106

Luo JY, Cui WJ, He P, Xia YY (2010) Raising the cycling stability of aqueous lithium-ion batteries by eliminating oxygen in the electrolyte. Nat Chem 2:760–765. https://doi.org/10.1038/nchem.763

Ma Z, Yu J, Dai S (2010) Preparation of inorganic materials using ionic liquids. Adv Mater 22:261–285. https://doi.org/10.1002/adma.200900603

Ma Z, Fan Y, Shao G, Wang G, Song J, Liu T (2015) In situ catalytic synthesis of high-graphitized carbon-coated $LiFePO_4$ nanoplates for superior Li-ion battery cathodes. ACS Appl Mater Interfaces 7:2937–2943. https://doi.org/10.1021/am5084368

Meng YS, Xia J, Zhu FL, Zhang Y (2016) Synthesis of N-doped carbon by microwave-assisted pyrolysis ionic liquid for lithium-ion batteries. Int J Electrochem Sci 11:9881–9890. https://doi.org/10.20964/2016.12.08

Meng Y, Han W, Zhang Z, Zhu F, Zhang Y, Wang D (2017) LiFePO4 particles coated with N-doped carbon membrane. J Nanosci Nanotechnol 17:2000–2005. https://doi.org/10.1166/jnn.2017.12869

Nakano H, Dokko K, Koizumi S, Tannai H, Kanamura K (2008) Hydrothermal synthesis of carbon-coated LiFePO[sub 4] and its application to lithium polymer battery. J Electrochem Soc 155:A909. https://doi.org/10.1149/1.2988048

Ni J, Morishita M, Kawabe Y, Watada M, Takeichi N, Sakai T (2010) Hydrothermal preparation of $LiFePO_4$ nanocrystals mediated by organic acid. J Power Sources 195:2877–2882. https://doi.org/10.1016/j.jpowsour.2009.11.017

Pei B, Wang Q, Zhang W, Yang Z, Chen M (2011) Enhanced performance of $LiFePO_4$ through hydrothermal synthesis coupled with carbon coating and cupric ion doping. Electrochim Acta 56:5667–5672. https://doi.org/10.1016/j.electacta.2011.04.024

Qie L et al (2012) Nitrogen-doped porous carbon nanofiber webs as anodes for lithium ion batteries with a superhigh capacity and rate capability. Adv Mater 24:2047–2050. https://doi.org/10.1002/adma.201104634

Ren L, Li X-E, Wang F-F, Han Y (2013a) Spindle $LiFePO_4$ particles as cathode of lithium-ion batteries synthesized by solvothermal method with glucose as auxiliary reductant. Rare Metals 34:731–737. https://doi.org/10.1007/s12598-013-0126-x

Ren W, Li D, Liu H, Mi R, Zhang Y, Dong L (2013b) Lithium storage performance of carbon nanotubes with different nitrogen contents as anodes in lithium ions batteries. Electrochimica Acta 105:75–82. https://doi.org/10.1016/j.electacta.2013.04.145

Shi Y, Chou S-L, Wang J-Z, Wexler D, Li H-J, Liu H-K, Wu Y (2012) Graphene wrapped $LiFePO_4$/C composites as cathode materials for Li-ion batteries with enhanced rate capability. J Mater Chem 22:16465–16470. https://doi.org/10.1039/c2jm32649c

Shin J-K, Lee CS, Lee K-R, Eun KY (2001) Effect of residual stress on the Raman-spectrum analysis of tetrahedral amorphous carbon films. Appl Phys Lett 78:631–633. https://doi.org/10.1063/1.1343840

Su J, Wu X-L, Yang C-P, Lee J-S, Kim J, Guo Y-G (2012) Self-assembled $LiFePO_4$/C nano/microspheres by using phytic acid as phosphorus source. J Phys Chem C 116:5019–5024. https://doi.org/10.1021/jp212063e

Sun C, Rajasekhara S, Goodenough JB, Zhou F (2011) Monodisperse porous $LiFePO_4$ microspheres for a high power Li-ion battery cathode. J Am Chem Soc 133:2132–2135. https://doi.org/10.1021/ja1110464

Sun X et al (2012) Enhanced electrochemical performance of $LiFePO_4$ cathode with in-situ chemical vapor deposition synthesized carbon nanotubes as conductor. J Power Sources 220:264–268. https://doi.org/10.1016/j.jpowsour.2012.07.082

Tang J et al (2013) Effect of transition metal on catalytic graphitization of ordered mesoporous carbon and Pt/metal oxide synergistic electrocatalytic performance. Microporous Mesoporous Mater 177:105–112. https://doi.org/10.1016/j.micromeso.2013.04.027

Wang X, Dai S (2010) Ionic liquids as versatile precursors for functionalized porous carbon and carbon-oxide composite materials by confined carbonization. Angew Chem Int Ed Engl 49:6664–6668. https://doi.org/10.1002/anie.201003163

Wang J, Sun X (2012) Understanding and recent development of carbon coating on LiFePO4cathode materials for lithium-ion batteries. Energy Environ Sci 5:5163–5185. https://doi.org/10.1039/c1ee01263k

Wang Y, Wang Y, Hosono E, Wang K, Zhou H (2008) The design of a $LiFePO_4$/carbon nanocomposite with a core-shell structure and its synthesis by an in situ polymerization restriction method. Angew Chem Int Ed Engl 47:7461–7465. https://doi.org/10.1002/anie.200802539

Wang J, Yang J, Tang Y, Li R, Liang G, Sham T-K, Sun X (2013a) Surface aging at olivine $LiFePO_4$: a direct visual observation of iron dissolution and the protection role of nano-carbon coating. J Mater Chem A 1:1579–1586. https://doi.org/10.1039/c2ta00521b

Wang L et al (2013b) Nano particle $LiFePO_4$ prepared by solvothermal process. J Power Sources 244:94–100. https://doi.org/10.1016/j.jpowsour.2013.03.101

Wang Q, Deng S, Wang H, Xie M, Liu J, Yan H (2013c) Hydrothermal synthesis of hierarchical $LiFePO_4$ microspheres for lithium ion battery. J Alloys Compd 553:69–74. https://doi.org/10.1016/j.jallcom.2012.11.041

Wu X-L, Jiang L-Y, Cao F-F, Guo Y-G, Wan L-J (2009) LiFePO4 nanoparticles embedded in a nanoporous carbon matrix: superior cathode material for electrochemical energy-storage devices. Adv Mater 21:2710–2714. https://doi.org/10.1002/adma.200802998

Xia Y, Zhang W, Huang H, Gan Y, Tian J, Tao X (2011) Self-assembled mesoporous $LiFePO_4$ with hierarchical spindle-like architectures for high-performance lithium-ion batteries. J Power Sources 196:5651–5658. https://doi.org/10.1016/j.jpowsour.2011.02.044

Xia J, Zhu F, Wang G, Wang L, Meng Y, Zhang Y (2017) Synthesis of LiFePO4/C using ionic liquid as carbon source for lithium ion batteries. Solid State Ionics 308:133–138. https://doi.org/10.1016/j.ssi.2017.06.007

Xie HM et al (2006) Optimized $LiFePO_4$–polyacene cathode material for lithium-ion batteries. Adv Mater 18:2609–2613. https://doi.org/10.1002/adma.200600578

Xu X, Xu Y, Zhang H, Ji M, Dong H (2015) The effect of NiO as graphitization catalyst on the structure and electrochemical performance of $LiFePO_4$/C cathode materials. Electrochim Acta 158:348–355. https://doi.org/10.1016/j.electacta.2015.01.170

Xu Z et al (2016) Migration behavior, oxidation state of iron and graphitization of carbon nanofibers for enhanced electrochemical performance of composite anodes. Electrochim Acta 222:385–392. https://doi.org/10.1016/j.electacta.2016.10.190

Xue H, Zhao J, Wang T, Guo H, Fan X, He J (2014) Facile and economical synthesis for "plum pudding"-shaped porous $LiFePO_4$/carbon composites for lithium ion batteries. RSC Adv 4:39400–39407. https://doi.org/10.1039/c4ra05342g

Yang J et al (2013) In situ self-catalyzed formation of core–shell $LiFePO_4$@CNT nanowires for high rate performance lithium-ion batteries. J Mater Chem A 1:7306–7311. https://doi.org/10.1039/c3ta11262d

Zhang W, Zhou X, Tao X, Huang H, Gan Y, Wang C (2010) In situ construction of carbon nano-interconnects between the $LiFePO_4$ grains using ultra low-cost asphalt. Electrochim Acta 55:2592–2596. https://doi.org/10.1016/j.electacta.2009.11.072

Zhang H, Xu Y, Zhao C, Yang X, Jiang Q (2012) Effects of carbon coating and metal ions doping on low temperature electrochemical properties of $LiFePO_4$ cathode material. Electrochim Acta 83:341–347. https://doi.org/10.1016/j.electacta.2012.07.128

Zhao T et al (2010) XAS study of $LiFePO_4$ synthesized by solid state reactions and hydrothermal method. Nuclear Inst & Methods in Physics Research A 619:122–127. https://doi.org/10.1016/j.nima.2010.01.066

Zheng Z, Pang WK, Tang X, Jia D, Huang Y, Guo Z (2015) Solvothermal synthesis and electrochemical performance of hollow $LiFePO_4$ nanoparticles. J Alloys Compd 640:95–100. https://doi.org/10.1016/j.jallcom.2015.04.007

Zhou N, Wang H-Y, Uchaker E, Zhang M, Liu S-Q, Liu Y-N, Cao G (2013) Additive-free solvothermal synthesis and Li-ion intercalation properties of dumbbell-shaped $LiFePO_4$/C mesocrystals. J Power Sources 239:103–110. https://doi.org/10.1016/j.jpowsour.2013.03.136